THESIS FOR THE DEGREE OF LICENTIATE OF ENGINEERING

ON THE COUPLING OF THE LOCALIZED PLASMON AND INTERBAND TRANSITIONS IN NICKEL NANOANTENNAS

Zhaleh Pirzadeh

Department of Applied Physics

CHALMERS UNIVERSITY OF TECHNOLOGY

Göteborg, Sweden 2013

On the coupling of the localized plasmon and interband transitions in
nickel nanoantennas

Zhaleh Pirzadeh

On the coupling of the localized plasmon and interband transitions in nickel nanoantennas

Zhaleh Pirzadeh
Department of Applied Physics
Chalmers University of Technology

Abstract

Interaction of light with metallic nanostructures smaller than the wavelength leads to excitation of collective oscillations of "free" conduction electrons. This effect leads to locally enhanced electric fields inside and outside the nanoparticle and is called localized surface plasmon resonance (LSPR). The history of this phenomenon goes back to 4th century where metallic nanoparticles were used to stain glass windows in medieval church windows. It was not until hundred years ago, however, that the physics behind the vibrant colors of noble metal nanoparticles was studied and understood - a development that ultimately resulted in the foundation of a new field in nanoscience, nanoplasmonics.

Nickel (Ni) is a transition metal, which is mainly used in the preparation of alloys due to its strength, ductility and resistance to corrosion and heat. In nanoplasmonics, this metal has so far received much less attention than the "classic" plasmonic metals such as gold or silver. This is mainly due to its high ohmic losses and electronic interband transitions, which induces large damping to its LSPR. However, since most metals feature local or broad interband transitions, it is crucial to gain deeper fundamental understanding of their interaction with the plasmonic excitations. As Ni features a spectrally localized interband transition at 4.7 eV is a very good "model system" to scrutinize the LSPR-interband transition interaction. The latter is crucial in view of an increasing number of metals being considered for nanoplasmonic applications.

In this thesis, the interaction between a spectrally localized interband transition and LSPR in nickel nanodisks is studied as a model system. This was done by spectrally tuning the LSPR by engineering of the nickel nanoantenna geometry or by tuning the refractive index of the surrounding medium. Using this approach, we show both experimentally and theoretically that the plasmon-interband interaction can be understood in the classical picture of two coupled harmonic oscillators, which approach a strong coupling regime. That is characterized by characteristic *"energy anticrossing"* behavior. These results can be generalized to all plasmonic metals, which feature spectrally localized interband transitions, and contribute to the general fundamental understanding of the role of interband transitions in plasmonic systems.

Keywords: Localized surface plasmon resonance, interband transition, nickel nanoplasmonic, coupling, nanoantenna

Appended paper

The following work is included in this thesis:

Paper I

Plasmon - Interband Coupling in Nickel Nanoantennas

Zhaleh Pirzadeh, Tavakol Pakizeh, Vladimir Miljkovic, Christoph Langhammer and Alexandre Dmitriev

Submitted for publication

Other publications

The following works are related but not included in this thesis:

Paper II

Plasmonic Nickel Nanoantennas

Jianing Chen, Pablo Albella, Zhaleh Pirzadeh, Pablo Alonso-González, Florian Huth, Stefano Bonetti, Valentina Bonanni, Johan Åkerman, Josep Nogués, Paolo Vavassori, Alexandre Dmitriev, Javier Aizpurua, and Rainer Hillenbrand
Small (2011), 7, No. 16, 2341–2347

Paper III

Designer Magnetoplasmonics with Nickel Nanoferromagnets

Valentina Bonanni, Stefano Bonetti, Tavakol Pakizeh, Zhaleh Pirzadeh, Jianing Chen, Josep Nogués, Paolo Vavassori, Rainer Hillenbrand, Johan Åkerman and Alexandre Dmitriev
Nano Letters 11 (2011) 5333–5338

Paper IV

Polarizability and Magnetoplasmonic Properties of Magnetic General Nanoellipsoids

Nicolò Maccaferri, Juan B. González-Díaz, Stefano Bonetti, Andreas Berger, Mikko Kataja, Sebastiaan van Dijken, Josep Nogués, Valentina Bonanni, Zhaleh Pirzadeh, Alexandre Dmitriev, Johan Åkerman and Paolo Vavassori.
Optics Express (2013), 21, No. 8, 9875-9889

Contents

1 Introduction

Nanoplasmonics is the field that deals with the research about localized surface plasmon resonance, a collective oscillation of free charge carriers in metallic nanostructures excited by near-visible light.

Although there was no scientific understanding of the optical properties of metallic nanoparticles before Faraday in the middle of the 19th century [1], the application of these particles dates much further back in time, when gold and silver nanoparticles were used in stained glass to create beautiful variation of colors in the windows of many churches. An impressive example of this application is presented in figure 1.1.a. Another example is the famous Lycurgus cup, crafted by a Roman glass artist in the 4th century, which manifests different color depending on whether it is illuminated from inside or outside as shown in figure 1.1.b. When the cup is illuminated from outside the scattered light from the incorporated nanoparticles defines the color of the cup and it appears greenish while, when illuminated from inside, the transmitted light determines the reddish color of the cup since shorter wavelengths are efficiently absorbed by the plasmonic particles.

Figure 1.1: Application of plasmonic nanoparticles dates far back in time, as exemplified by the gothic stained glass rose window of the Notre-Dame de Paris cathedral (left most). The colors are created by colloidal gold nanoparticles in the glass. (b) The Lycurgus cup, crafted by a Roman artist in the 4th century is another example of early application of plasmonic nanoparticles [2]. In the picture it is shown that, when illuminated from outside, the scattering of light from the particles determines the color of the cup and it appears green (middle), on the other hand, when illuminated from inside it's the light transmitted through the particles that gives rise to the color of the cup, which appears to be red since shorter wavelengths are absorbed by the particles (right most).

The optical properties of metallic nanostructures were not explained theoretically until the 20th century when Mie found an analytical solution for the Maxwell equation, which could describe the light absorption and scattering of spherical metallic nanoparticles [3]. During the last decades numerical methods have been developed, which now make it possible to, on a daily basis, calculate both the near and far field optical properties of nanoparticles with much more complex shapes [4]. Examples of such methods are the discrete dipole approximation (DDA) [5] or the

finite difference time domain (FDTD) method [6], which was used for the purpose of calculating near-field enhancements in the appended paper.

When it comes to plasmonic materials, nickel has not been considered very interesting due to its high ohmic losses [7,8]. Bound electron transitions, i.e. interband transitions, have been considered unfavorable due to their optical absorption in the visible range of the electromagnetic spectrum, which can interfere with the plasmonic response. This is why the "classic" metals used in in the plasmonics field are the ones that have their plasmonic response spectrally well separated from their bound electron transitions, i.e. Au, Ag and Al.

In this thesis, I take another perspective on interfering plasmon resonance with interband transitions by investigating in a systematical way, how an LSPR mode couples spectrally to a localized interband transition. It has been reported that the plasmonic response of palladium nanoparticles is strongly governed by Fano-interference with a broad interband transition background [9,10,11]. Nickel, which is the focus of my work presented here, has a rather sharp and spectrally localized interband transition [12,13], which can interact strongly with the plasmon excitation and give rise to new optical properties that are different than a simple linear combination of the two constituents [14-18]. Therefore, linking localized plasmons with interband transition can be regarded as a new approach to tailor optical properties of materials. Specifically, in this thesis I studied the interaction between the localized plasmon resonance (LSPR) and interband transition in nickel nanostructures. I demonstrate both experimentally and theoretically that plasmons strongly couple to interband transitions in metallic nanostructures. The coupling gives rise to interesting effects like energy anti-crossing of the interband transition and plasmon mode. The generated phenomenological concept can be applied to other metals with their local bound transition in the UV-VIS range of electromagnetic spectrum such as Al, Cu and Fe [12,13].

The outline of this thesis is such that chapter 2 gives a brief introduction to optical properties of metals, basics of electronic band structure and the Drude-Lorentz model. Chapter 3 presents an overview of concepts such as dielectric function, polarizability, absorption/scattering/extinction efficiencies as well as absorption enhancement. Chapter 4 describes the nanofabrication method used for the production of the samples in this thesis. Chapter 5 provides an overview of different characterization methods used to study the sample's optical properties as well as topology and actual structure. Finally, chapter 6 summarizes the appended paper and gives an outlook for future work.

2   Optical properties of metals

In order to understand the behavior of different metals, one can look at their band structure. The band structure describes the range of different energy states that electrons can occupy in the material [19]. The energy of these states is given by the Schrödinger equation for the motion of the electron in a periodic potential imposed by the lattice structure. At room temperature, when a material is excited by an external electric field, electrons can occupy these states up to a certain level of energy and the states above that energy will be left empty. This specific energy level is called Fermi energy (E_f) [19-21]. Another important concept in the band structure of materials is the band gap, which is a certain region of energy that cannot be occupied by electrons. This is the reason why some materials are efficient in conducting electrons and some are not [22].

The size of the band gap as well as its energy with respect to the Fermi energy is the key concept to differentiate between metals, semiconductors and insulators [23]. Schematics of Fermi level position in relation to the band gap in these different material classes is presented in figure 2.1.
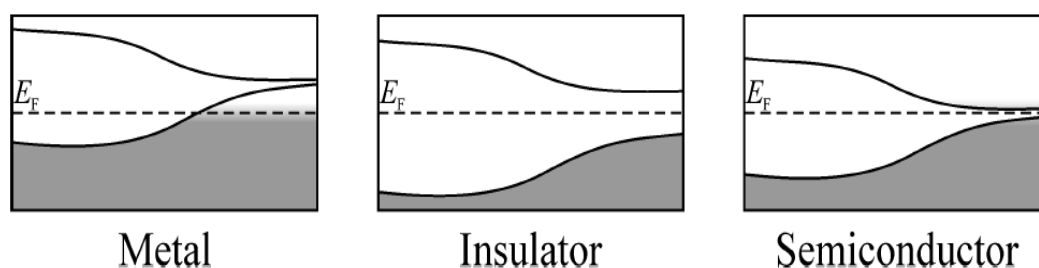

Figure 2.1: Schematics of band structure of different materials. Fermi level is located inside a band in metals where for insulators and semiconductors the Fermi level is inside the band gap. For the semiconductors however, the band gap is narrow enough to be overcome by applying an external heating, doping or an electric field [20,23].

As it can be seen in this figure, for metals, the Fermi energy crosses the conduction band, which makes it possible for the electrons to move back and forth freely, while for the insulator and semiconductors the Fermi energy is located inside the band gap, which means the electron needs to absorb some energy to overcome the gap and get excited to the conduction band. For the case of semiconductors the gap size is small enough to be overcome by exciting electrons with similar energy to the band gap, where as for the insulators this is not the case. This explains why metals are such good electrical conductors while insulators don't conduct electrons [20,22].

2.1   Electronic transitions and band structure

The electronic band structure shows the allowed electronic transitions inside a material. Electronic transitions are the event when an electron from a filled state below the Fermi level is excited to an empty state above the Fermi level [19]. Such an excitation can occur either inside the same band (intra-band transition) or from one band to another (interband transition). In these transitions the electron energy and/or momentum can be changed. When the electron transfers to another energy level

without changing momentum, it's a direct transition, while, when both energy and the direction of the electron change, it's an indirect transition. However, mostly a photon in the visible range does not have enough momentum to change the momentum of the electron and thus the direct transitions are mostly the dominant ones [24]. All these transitions contribute to absorption of light, which manifests itself in the optical response of the metals. A sketch of different types of electronic transitions is presented in figure 2.2.
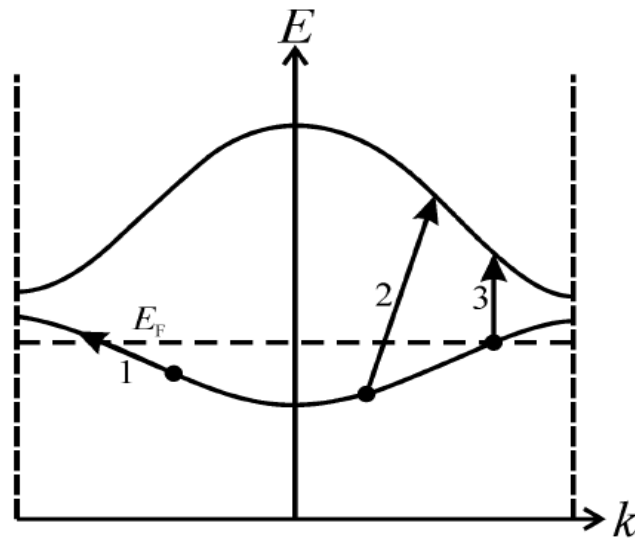

Figure 2.2: Schematics of different types of electronic transition in metals. The first arrow shows an intraband transition within the same band, where number 2 and 3 show indirect and direct interband transitions, respectively. [24]

The band structure and the density of states (DOS) of nickel are displayed in figure 2.3 [24,25]. The outer electrons of this metal belong to the 3d and 4s bands, which are in the vicinity of the Fermi level. As it can be seen in this figure, at some certain energy (gray area), the metal has much higher DOS, which corresponds to the d-band that is fairly close to the Fermi energy and plays a crucial role in the optical properties of nickel.
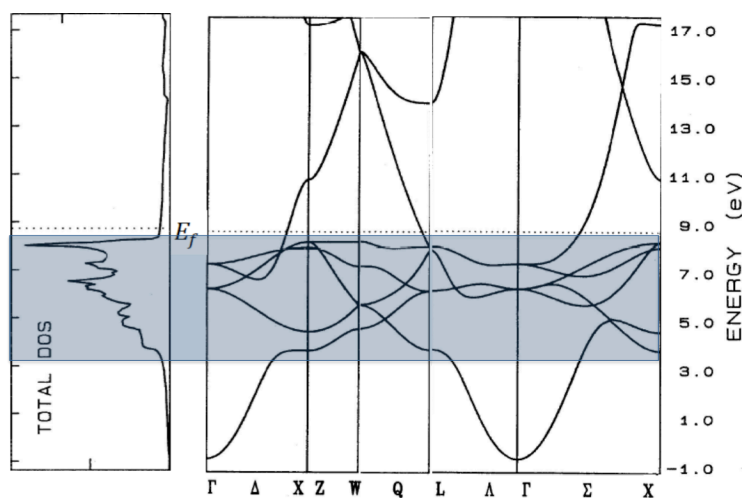

Figure 2.3: Density of states (DOS) and band structure of nickel. In the DOS figure, the gray region corresponds to the d band, which is very close to the Fermi energy as it can be seen in this figure [24].

2.2 Drude-Lorentz model

The interactions of metals with electromagnetic radiation, i.e. their optical properties, are wavelength dependent and can be conveniently described by the complex dielectric function:

$$\varepsilon(\omega) = \varepsilon'(\omega) + i\varepsilon''(\omega) \tag{2.1}$$

The dielectric function describes how an electric field affects and is affected by a medium and as it can be seen in equation 2.1, consists of two parts. The first term is the real part of the dielectric function, which is related to the stored energy within the medium. The second term is the imaginary part of the dielectric function and relates to absorption (loss) of energy within the medium. Under certain conditions, when the frequency of the external alternating electric field matches the natural frequency of metal surface electrons, one can induce a cooperative collective oscillation of the free electrons in the system, a so-called plasmon resonance.

To describe the response of a single electron, Lorentz used a simple model where electrons are considered as "damped" harmonically bound particles that are subject to an external electric field [26]. A simple picture of this model is to assume the electron as a small mass that is connected to its atom by a spring. Thus the material can be approximated as an ensemble of harmonic oscillators. The motion of a bound electron in an oscillating electric field can then be described as:

$$m_e \frac{\partial^2 r}{\partial t^2} + \gamma \frac{\partial r}{\partial t} + k.r = eE_0 \, e^{-i\omega t} \tag{2.2}$$

where m_e is the mass of the electron, γ is the damping factor and k is a restoring force. This leads to a dielectric function described by

$$\varepsilon(\omega) = 1 + \frac{G_0 \omega_0^2}{\omega_0^2 - \omega^2 - i\Gamma\omega} \tag{2.3}$$

where $\omega_0 = \sqrt{\frac{k}{m_e}}$, G_0 and $\Gamma = \frac{\gamma}{m_e}$ are the Lorentz central frequency, amplitude and damping factor, respectively [4,26,27]. However, for a free electron scenario where $k = 0$, the dielectric function becomes:

$$\varepsilon(\omega) = 1 - \frac{\omega_p^2}{\omega^2 + i\gamma\omega} \tag{2.4}$$

where ω_p is the bulk plasma frequency, which is dependent on the electron density of the material through

$$\omega_p = \sqrt{\frac{ne^2}{m_e \epsilon_0}} \tag{2.5}$$

where n is the electron density and ϵ_0 is the permittivity of vacuum. The Drude model is efficient for approximating the dielectric function of metals without considering the electrons from the bound states [28,29], i.e. to describe a free-electron metal.

If we now want to describe the optical properties of a real metal and take both the free and bound electron contributions into account, we combine the concepts put forward by Drude and Lorentz in the so-called Drude-Lorentz model of the metal dielectric function, resulting in:

$$\varepsilon(\omega) = E_{dc} - \frac{\omega_p^2}{\omega^2 + i\gamma\omega} + \frac{G_0\omega_0^2}{\omega_0^2 - \omega^2 - i\Gamma\omega} \tag{2.6}$$

where the first two terms correspond to the Drude (free electron) model and the third term corresponds to the Lorentz (bound electron) model [4,16]. Here we consider a special case where we have only one interband transition. However, for optical properties of the metal is also influenced from the other interband transitions happening in much higher energies. This is taken into account by introducing E_{dc}, which compensates for the contribution of interband transitions at higher energies. This model, together with the Modified Long Wavelength Approximation (MLWA, see chapter 3), was used in my work to calculate the dielectric function and optical properties (extinction, absorption and scattering) of nickel nanodisks. An example of such calculations is shown in figure 2.4, where we first calculated the dielectric function based on the free electron and bound electron model separately, and then combined both models to derive the Drude-Lorentz dielectric function.
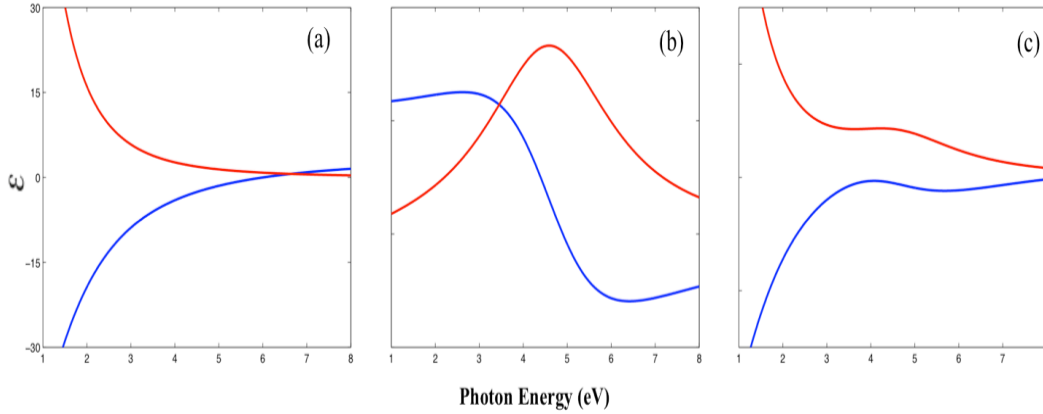

Figure 2.4: Dielectric function of nickel calculated by Drude model (a), Lorentz model (b) and Drude-Lorentz model (c). $E_{dc} = 3.6\ eV$, $\omega_p = 11.7$ eV, $\gamma = 1.4$ eV, $G_0 = 4.6$, $\omega_0 = 4,9$ eV and $\Gamma = 3.5$ eV.

3   Nanoplasmonics

So far I have only described the optical properties of bulk metals without focusing on nanostructures, and how light (electromagnetic waves) interacts with the latter. Thus, in this chapter, I will discuss what localized surface plasmon resonance (LSPR) is and introduce the basic concepts used in the nanoplasmonics field to explain the optical response of metal nanoparticles. Finally, I will give a brief explanation of the antenna effect in optical absorption of nickel nanodisks.

3.1   Localized surface plasmon resonance

When a metallic nanoparticle is illuminated by light with a wavelength longer or comparable to the size of the nanoparticle, a collective oscillation of the free electrons in the metallic nanostructure is excited, which is called the localized surface plasmon resonance. During this oscillation, the conduction electrons are spatially separated from the metal positive ions at the particle boundaries, which gives rise to highly localized charge separation [20] with the following consequences:

I.   The electric near field at the particle surface is strongly enhanced with respect to the incoming (light) field that excites the resonance. The largest enhancement is found right at the surface of the particle and decays exponentially with distance ($\frac{1}{r^3}$ where r is the distance) [27,30].

II. In the far field the maximal extinction of light by the plasmonic particle occurs at the plasmon resonance frequency. This extinction maximum is manifested by a "peak" in the extinction spectrum, which indicates the LSPR frequency. The latter is generally located in the near-visible range and depends on the size, the shape, and the dielectric function of the particle (i.e. what material they are made of), as well as the dielectric function of the surrounding environment [4,27,31].

In order to calculate optical properties of metallic nanostructures, a simple analytical model, called dipole approximation, can be used for spheroidal nanoparticles. This model makes two main simplifying assumptions. First that the electric field incident on the particle is constant in time and space, and second that the size of the particle is much smaller than the wavelength of the incident light. Based on these assumptions the dipole moment (p) of a particle subjected to an electric field E_0 is:

$$p = \varepsilon_m \alpha E_o \tag{3.1}$$

where ε_m is the dielectric function of the medium the particles are immersed in and α is the polarizability of the particle. For a spherical particle with radius a and dielectric function ε_1, the polarizability can be calculated as:

$$\alpha = 4\pi a^3 \frac{\varepsilon_1 - \varepsilon_m}{\varepsilon_1 + 2\varepsilon_m} \tag{3.2}$$

if the electric field is not constant i.e. varying with time, the cross section of extinction, scattering and absorption can be calculated as:

$$C_{ext} = 4\pi ka^3 Im\left\{\frac{\varepsilon_1 - \varepsilon_m}{\varepsilon_1 + 2\varepsilon_m}\right\} \tag{3.3}$$

$$C_{sca} = \frac{8\pi}{3}k^4 a^6 \left|\frac{\varepsilon_1 - \varepsilon_m}{\varepsilon_1 + 2\varepsilon_m}\right|^2 \tag{3.4}$$

$$C_{abs} = C_{ext} - C_{sca} \tag{3.5}$$

From these equations it can be seen that a resonance will occur when the extinction or scattering cross section is maximized, i.e. under the resonance condition:

$$\varepsilon_1 = -2\varepsilon_m \tag{3.6}$$

Assuming that the spherical particle is metallic, one can describe the dielectric function, in a first approximation, by the Drude model introduced above:

$$\varepsilon_1 = 1 - \frac{\omega_p^2}{\omega^2 + i\gamma\omega} \tag{3.7}$$

where ω_p is the bulk plasma frequency and γ is the damping factor. Combining this equation with the previous one, we obtain the LSPR frequency (ω) or wavelength (λ) [29] of a Drude nanoparticle as:

$$\omega_{max} = \frac{\omega_p}{\sqrt{2\varepsilon_m + 1}} \tag{3.8}$$

$$\lambda_{max} = \lambda_p\sqrt{2\varepsilon_m + 1} \tag{3.9}$$

An example of such a calculation is presented in figure 3.1(a, c) where the dielectric function of gold and nickel are calculated based on the Drude model with Drude parameters of omega=8.55 eV and gamma=0.0184 eV for gold and omega = 11.7 eV and gamma = 1.4 eV for nickel (dashed lines). For comparison, the experimentally determined dielectric functions for both metals taken from Palik and Johnsson Christy, respectively, are also plotted (solid lines) [12,13]. As it can be seen in this figure, the Drude model cannot count for the interband transition at higher energies. This is why one needs to take the bound electron contribution into account as well when studying the optical properties of metals. The latter is done by adding Lorentz terms to describe the interband transitions. The calculated plasmon response of a gold/nickel sphere with diameter 60 nm is also shown in figure 3.1(b, d) based on both experimental data for the dielectric function and calculations using Drude model. As it can be seen in the plasmonic response of these two metals, nickel shows broader response that spans across a wide range of the electromagnetic spectrum compared to the one from gold. This can be explained by ohmic losses and non-radiative damping where the decay of the LSPR excites electron-hole pairs, which via phonon coupling, results in heating of the particle [7,20].
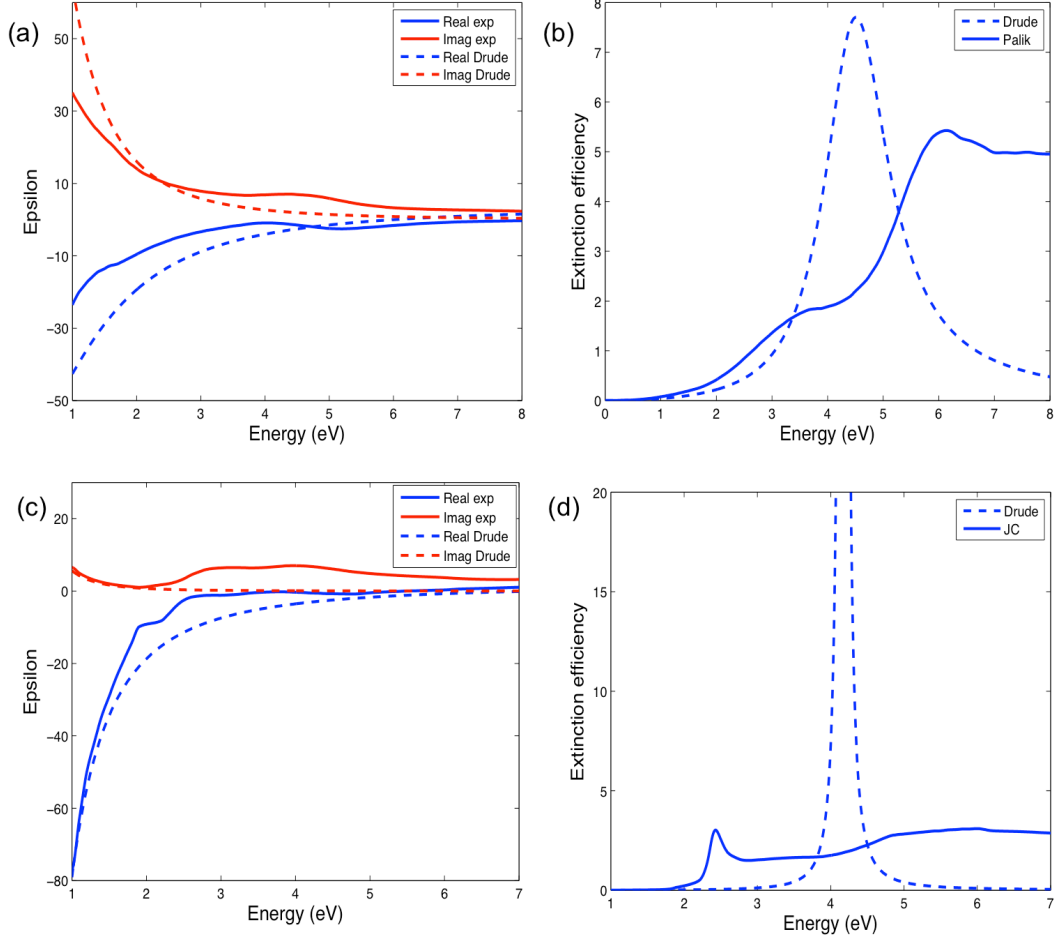
Figure 3.1: a, c) Dielectric function of nickel and gold, respectively based on experimental data taken from Palik [13] (solid line) and calculation by Drude model (dashed line) and in b, d) the plasmonic response of a nickel and gold sphere respectively, with diameter 60 nm is calculated based on experimental data from Palik (solid line) and Drude model (dashed line).

3.2 Modified long wavelength approximation

When the size of a metallic nanoparticle is increased (i.e. it becomes comparable to the wavelength of the incoming light), the electric field along the particle is not constant any longer, which means that the electrons in the particle no longer are homogeneously polarized. Experimentally this is manifested in a spectral red-shift and broadening of the resonance. To account for this so-called dynamic depolarization, the Modified Long Wavelength Approximation (MLWA) [32,33] of the dipole model introduced above can be efficiently used for ellipsoidal particles. In the MLWA the particle dipole moment is modified to:

$$p = \alpha(E + E_{rad}) \qquad (3.10)$$

where E_{rad} accounts for depolarization of the field and is given by:

$$E_{rad} = \frac{2}{3}ik^3p + \frac{k^2}{a}p \qquad (3.11)$$

9

The first term accounts for radiative damping through increased scattering whereas the second term accounts for the dynamic depolarization effect. The dipole polarizability of a spheroidal particle becomes:

$$\alpha_i = 4\pi abc \frac{\varepsilon_1 - \varepsilon_m}{3\varepsilon_m + 3L_i(\varepsilon_1 - \varepsilon_m)} \tag{3.12}$$

where L_i is a shape factor to account for the modification of the dipole along each axis due to the shape of the particle. It is given by:

$$L_i = \frac{abc}{2} \int_0^\infty \frac{dq}{(s_i^2 + q)\sqrt{(q + a^2)(q + b^2)(q + c^2)}} \tag{3.13}$$

which for sphere (a = b = c) L_i=1/3, result in the polarizability given in equation 3.2. The modified MLWA polarizability that accounts for the non-uniform electrical field due to finite size effect is then calculated by [34]:

$$\alpha_{MLWA} = \frac{\alpha_i}{1 - \frac{2}{3}ik^3\alpha_i + \frac{k^2}{a}\alpha_i} \tag{3.14}$$

Here, I have used the MLWA to calculate the plasmonic response of my nickel nanodisk arrays of diameter 60 nm and thickness of 20 nm by approximating the disks as oblate spheroids (a = b ≠ c) embedded in effective medium with a refractive index averaging over the one of glass (1.5) and air (1) shown in dashed lines in figure 3.2. For comparison, the measured spectrum for the same nickel nanodisk array is also plotted (solid line). As it can be seen in this figure there is a good agreement between experimental measurements and MLWA calculations with minor difference in absolute values of extinction efficiency.
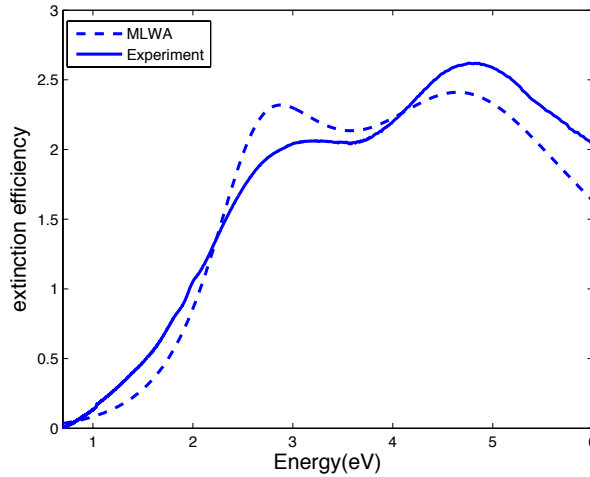

Figure 3.2: Experimentally measured and MLWA calculated optical extinction of nickel nanodisks with diameter of 60 nm and thickness of 20 nm.

As mentioned earlier in equation 3.9, the LSPR resonance frequency (wavelength) is dependent on the dielectric function of the surrounding medium ε_m. Thus one can think of utilizing this resonance as a sensing tool to sense the changes in or around the nanoparticles through tracking the LSPR position before and after the change. This opens the door to many sensing applications in the nanoplasmonics field [35-37]. The sensitivity of LSPR to the refractive index (RI) of the surrounding medium was used in this thesis to shift the plasmon resonance to lower energies compared to a spectrally localized interband transition in nickel. This was done by evaporating a thin (20 nm) film of SiO_2 on top of the original sample, i.e. nickel nanodisks of diameter 60 nm and thickness 20 nm. This results in embedded structures in higher RI (1.5) compared to the original sample surrounded by air RI (1.25) and thus a red-shift of the plasmon resonance to lower energies, as can be seen in figure 3.3.
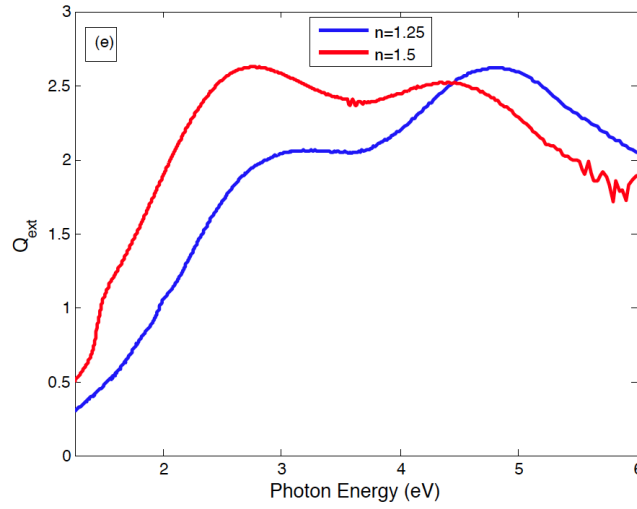

Figure 3.3: Optical response of nickel disk with diameter 60 nm and thickness 20 nm before (blue) and after silica deposition.

3.3 Antenna effect in the optical absorption

As mentioned earlier, the electric dipole approximation of the plasmonic nanoparticles can be used to calculate the scattering, absorption and extinction cross-sections of metallic particles. The rate of the absorbed energy can be calculated by

$$P = \sigma_A I_0 \qquad (3.15)$$

where P is the rate of absorbed energy in the particle per unit time (W=J/s), σ_A is the absorption cross-section (m^2) and I_0 is the intensity of the incident light (W/m^2). The rate of energy absorbed in the particle can also be calculated as [38]

$$P = \frac{\omega}{2} \iiint \varepsilon''(\omega) E_L(r, \omega) . E_L^*(r, \omega) \partial^3 r \qquad (3.16)$$

where $\varepsilon''(\omega)$ is the imaginary part of the dielectric function of the particle and $E_L(r, \omega)$ is the local electric field and depends on both wavelength and the position (r) and the integration runs over the volume of the particle [38-41]. We also have

$$I_0 = \frac{1}{2} c_0 |E_0|^2 \tag{3.17.a}$$

$$I_L(r) = \frac{1}{2} c_0 |E_L(r)|^2 \tag{3.17.b}$$

$$|E_L(r)|^2 = E_L(r) \cdot E_L^*(r) \tag{3.17.c}$$

where c_0 is the speed of light and I_L is the intensity of the local electric field inside the particle. Now combining equations 3.15 and 3.16 gives us:

$$P = \frac{\omega}{c_0} \varepsilon''(\omega) \iiint I_L(r) \partial^3 r \tag{3.18}$$

Now if we define the field enhancement factor (M) as the ratio between the amplitude of the local electric field in the particle over the amplitude of the incident electric field. This is the same as the ratio between the intensities, respectively.

$$M(r) = \frac{|E_L(r)|}{|E_0|} \tag{3.19}$$

$$M^2(r) = \frac{I_L(r)}{I_0} \tag{3.20}$$

Thus we will have the absorbed energy rate as

$$P = \frac{\omega}{c_0} \varepsilon''(\omega) I_0 \iiint M^2(r) \partial^3 r \tag{3.21.a}$$

$$P = \frac{\omega}{c_0} \varepsilon''(\omega) I_0 \overline{M^2} V \tag{3.21.b}$$

where $\overline{M}$ is the average field enhancement factor and can be calculated by

$$\overline{M^2} = \frac{c_0 \sigma_A}{\omega \varepsilon'' V} \tag{3.22}$$

To study how the absorption is enhanced inside the nickel nanoparticles we use this near-field concept in a reverse approach. Here, we used the absorption cross-section σ_A that was calculated by DL model using MLWA approximation and divided this over the volume of the nanodisks and the imaginary part of nickel dielectric function to derive the average field enhancement factor. An example of such calculation is presented in figure 3.4 for nickel nanodisks of various diameters (190 nm -10 nm) and thickness of 20 nm. The first graph shows the absorption cross-section calculated by the DL model using MLWA. The second graph shows when the absorption cross-section is divided by the geometrical area of the nickel nanodisks yielding absorption efficiency. Finally the last graph shows the result of dividing absorption cross-section by the volume of nickel nanodisks and imaginary part of the dielectric function of nickel yielding the antenna factor (M) as shown, i.e. how well the absorption is enhanced due to LSPR in the nickel nanodisks. Phenomenologically, this

enhancement can be understood as the LSPR "forcing" the light to stay longer in the material and thus giving it more time to be absorbed.
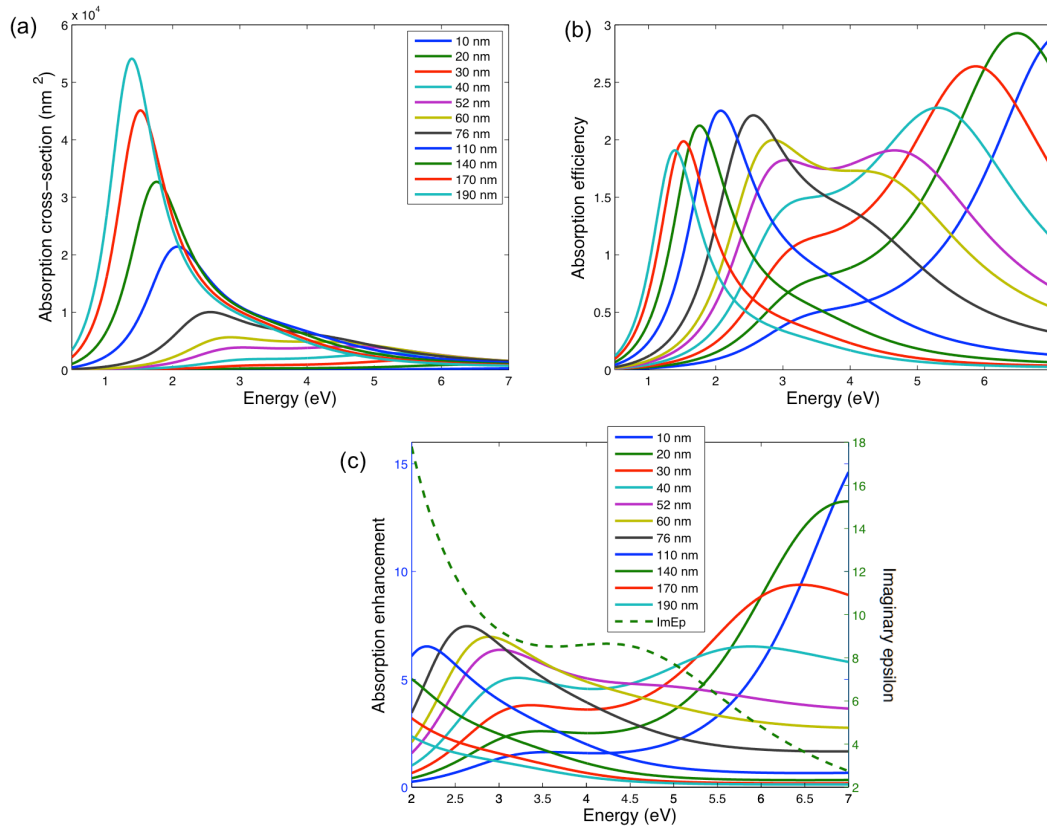

Figure 3.4: Antenna effect in optical absorption of nickel nanodisks of various diameters (190-10 nm) and thickness of 20 nm. a) absorption cross-section, b) absorption cross-section divided by geometrical area of the nanodisk (absorption efficiency) and c) the antenna factor, the absorption cross-section divided by the nanodisk volume and imaginary part of dielectric function of nickel.

As it can be seen in figure 3.4 the antenna factor is enhanced when the diameter of the nickel nanodisk was decreased from 190 nm to 10 nm. The same results can be obtained by changing the refractive index of the surrounding medium as mentioned earlier to tune LSPR spectrally.

3.4 Two coupled harmonic oscillators

So far, it has been described how the optical properties of metallic nanoparticles depend on the interaction of their bound and free electron with the incident light. The Drude-Lorentz model was introduced to calculate the dielectric function of metallic nanostructures combining the free (Drude) and bound (Lorentz) electron contributions. However, the interaction between these two in the particle has not been explained yet. In this section I try to describe this interaction by introducing the two coupled harmonic oscillator concept, deriving the motion of electrons and eigenfrequencies in such a coupled system.

Although the dominant factor in the optical response of metallic nanoparticles in the visible spectral range in due to the free electron contribution, the interband transitions also affect the interaction between these particles and incoming light noticeably. The

13

interaction between the plasmonic response of nickel nanodisks and an interband transition (IBT) can be described by a classical two coupled harmonic oscillator model, as described by Novotny [42] where IBT (bound electron contribution) is associated with oscillator A with spring constant of k_A, and the plasmonic response (free electron contribution) is associated with oscillator B with spring constant k_B as shown in figure 3.5. This is reasonable due to oscillator nature of the dielectric function, i.e. that it can be well described by a Drude term for plasmon response and Lorentz term(s) for IBT. This system will then have two eigenfrequencies. When there is no coupling between these two oscillators ($\kappa=0$), we have the eigenfrequencies of $\omega_A = \sqrt{K_A/m_A}$ and $\omega_B = \sqrt{K_B/m_B}$. However when these two oscillators are coupled ($\kappa\neq0$) the motion of the electron can be described by

$$m_A x_A'' + K_A x_A + \kappa(x_A - x_B) = 0 \tag{3.23.a}$$

$$m_B x_B'' + K_B x_B + \kappa(x_A - x_B) = 0 \tag{3.23.b}$$

the solution to this homogenous system of equations results in new eigenfrequencies

$$\omega_\pm^2 = \frac{1}{2}\left[\omega_A^2 + \omega_B^2 \pm \sqrt{(\omega_A^2 + \omega_B^2)^2 + 4\Gamma^2\omega_A\omega_B}\right] \tag{3.24}$$

where

$$\omega_A = \sqrt{(K_A + \kappa)/m_A} \tag{3.25}$$

$$\omega_B = \sqrt{(K_B + \kappa)/m_B} \tag{3.26}$$

$$\Gamma = \frac{\sqrt{\kappa/m_A}\sqrt{\kappa/m_B}}{\sqrt{\omega_A/\omega_B}} \tag{3.27}$$

m_A and m_B are the mass of the two oscillators, k_A and k_B are their spring constants and κ is the coupling between the two.
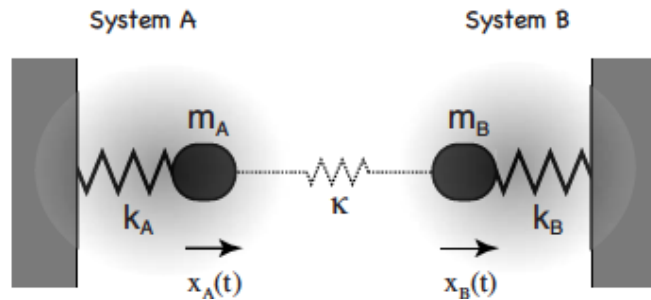
Figure 3.5: Schematic of two coupled harmonic oscillators with spring constants K_i and mass m_i and coupling factor of κ, where system A represents the Lorentz term for an interband transition, and system B represents the Drude term for the plasmon response of a metallic nanostructure [42].

In our case, we associate oscillator B to the plasmon response of nickel nanodisks and oscillator A to the IBT of these structures. Since the interband transition is given by

the band structure of nickel only, $k_A = k_0$ is set constant while one can easily change k_B through varying the size of nickel disks or the refractive index of the surrounding medium since this spring constant associated with plasmonic response of nickel nanodisk. In this way, one can study this interaction on an uncoupled system where the plasmon and IBT response are spectrally well separated. This is the case for larger nanodisks or higher refractive index of the surrounding medium. However, when the size of the nanodisks or the refractive index is decreased, these two systems start to interact in the form of a two coupled harmonic oscillators resulting in new frequencies that are different from the original frequencies before coupling. Through engineering the nickel nanodisk system, we can control this coupling and approach a strongly coupled regime with a characteristic fingerprint of an *"anticrossing"* region, which is a distinct frequency split where the two frequencies don't intersect anymore (as was the case for the uncoupled system). This interaction is studied in detail for nickel nanodisks of various sizes and refractive index in the appended paper.

4 Nanofabrication

The nanofabrication technique used for fabrication of the samples in this project is hole-mask colloidal lithography (HCL). HCL is a very efficient technique that can be used to produce large amorphous arrays of nanoparticles without long-range order by means of self- assembly during the mask fabrication step. In this chapter, I will first describe the different steps of HCL fabrication in detail, and then explain how the specific samples used for this project were fabricated.

4.1 Hole-mask colloidal lithography (HCL)

As mentioned earlier HCL can be used for fabrication of large area (cm^2) arrays of nanoparticles of various shapes, sizes and materials with the specific characteristic of a lack of long-range order [43]. The main feature that makes this method different from conventional colloidal lithography [36] fabrication methods is a sacrificial polymer layer (to facilitate lift-off) covered with a thin metal film perforated by nanoholes that can be used later as an evaporation mask. The sacrificial layer will be dissolved in an organic solvent during the lift off process, thereby removing all extra layers and leaving the desired pattern on the surface. Here I describe step-by-step how HCL samples are made. Figure 5.1 also presents schematic sketches of each step.

1. The first step is to cover the flat surface of the substrate (glass, fused silica, Si wafer) with a thin homogeneous sacrificial PMMA layer by spin coating. The thickness of PMMA depends on the viscosity of the polymer solution used as well as the rotation speed during the spin coating process (the faster the thinner).

2. After covering the substrate with PMMA, it is soft-baked either in an oven or on a hot plate at 180°C for 10 minutes in order to remove remaining solvent from the polymer layer. This is followed by a mild and short (3s) oxygen plasma etch to increase the hydrophilicity of the PMMA surface, which is crucial for the next steps.

3. To achieve the appropriate surface charge of the PMMA for the subsequent step, a monolayer of positively charged polyelectrolyte, Polydiallyldimethylammonium (PDDA), is deposited onto the sample through pipetting the solution on the surface and letting it incubate for a certain amount of time. After incubation, the sample is rinsed with de-ionized water, followed by blow-drying in a nitrogen stream. Now the substrate is positively charged (in water) and can be used as a basis for self-assembly of negatively charged Polystyrene nanoparticles in the next step.

4. In this step we pipet an aqueous suspension of negatively charged polystyrene colloidal particles onto the positively charged substrate for self-assembly. Due to the electrostatic repulsion between the particles themselves and the attraction between negatively charged particles and the positively charged surface, a sparse monolayer of particles will be formed on the surface, following a typical random-sequential-adsorption process. The substrate is rinsed again with de-ionized water and dried off in a stream of nitrogen to

remove excess colloids on the surface and prevent any rearrangements of the particles due to capillary force during drying process.

5. Now we have a surface with PS particles. A thin metal film is then evaporated onto the PS particle-decorated surface. This metal film will, in a later step, be used as evaporation mask and should be able to withstand oxygen plasma etching later in the process. Therefore the mask layer is typically made from Au or Cr.

6. In this step, after the metal film evaporation, the PS particles are removed by a simple tape-stripping procedure. For successful stripping it is important to assure a good contact between surface and tape and to avoid air bubbles. After removing the tape (on which the PS particles now are stuck) the metal mask layer is remaining on the sample surface but now perforated by nanoholes with a diameter corresponding to the one of the PS nanoparticle. This "hole-mask", resting on the sacrificial PMMA layer, can now be used as a mask for the main evaporation step.

7. Reactive oxygen plasma etching is now used to etch the PMMA layer where it is exposed in the nanoholes in the mask layer. In this way, the mask is "developed" in such a way that the substrate material becomes exposed in the nanoholes. The duration of etching as well as the gas used will determine the shape and size of the holes used as a mask for the main evaporation. For example, oxygen plasma is used to etch through the PMMA layer only where CF_4 can be used to etch through both sacrificial layer as well as the substrate for fabrication of embedded structures. With this technique we can produce various types of structures such as nanodisks, nano-ellipses, nano-cones and dimers.

8. In the second-last-fabrication step the material, from which the targeted nanostructures should consist of, is evaporated into the nanoholes that are now used as evaporation mask. This can be a single material evaporation, or successive evaporations to produce different layers of materials such as nanosandwiches, dimers, etc.

9. The last step is to remove the excess evaporated material as well as the PMMA and the mask layer by sonication of the sample in acetone. In this lift-off step, the PMMA is dissolved in the acetone and will thus carry along all the material layers resting on top of it. This will finally leave the sample surface covered with the desired nanostructures only. The surface is rinsed with de-ionized water and blow dried with nitrogen at the end.
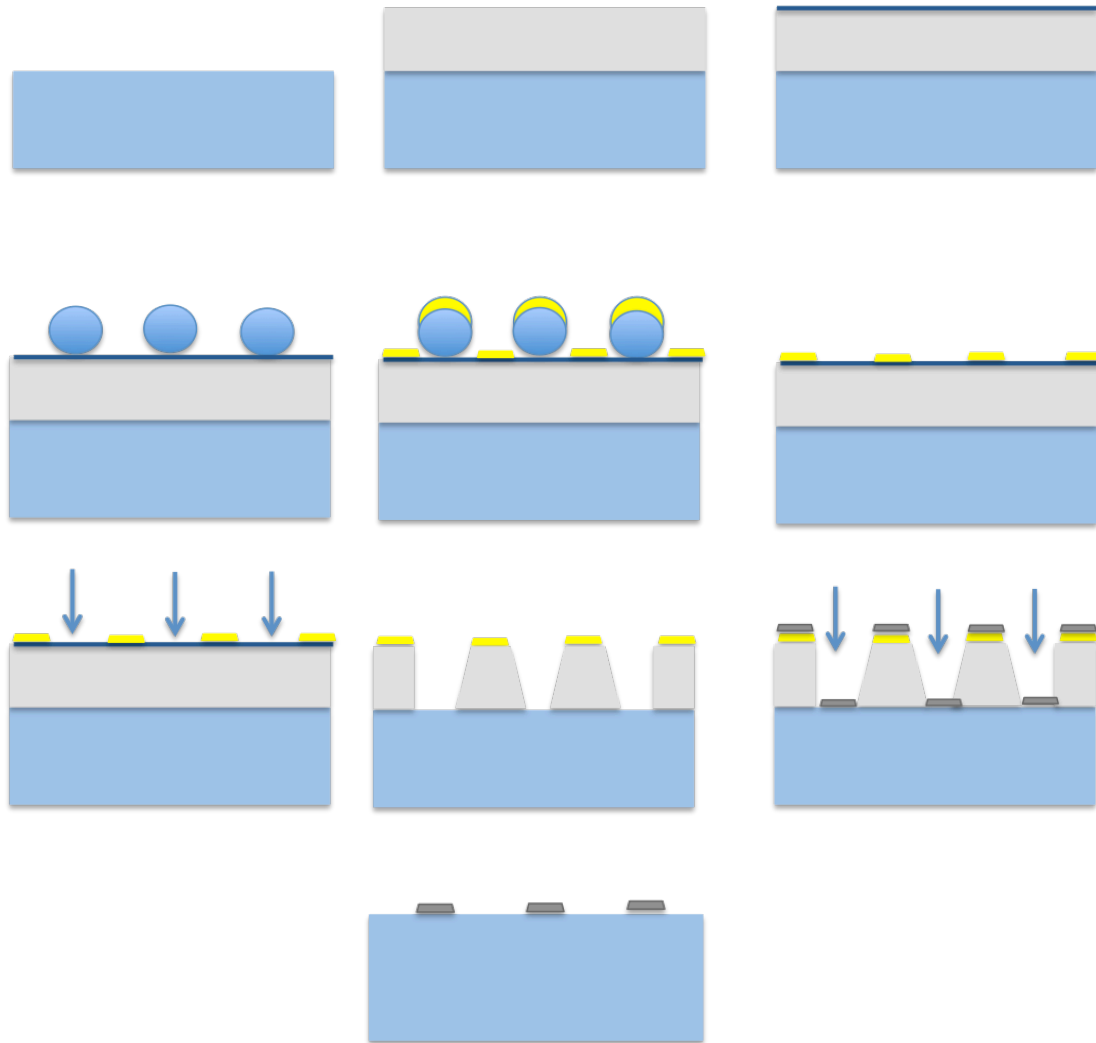
Figure 4.1: HCL fabrication method step-by-step: glass surface, covered by PMMA then covered by a positively charged polyelectrolyte nanolayer and negatively charged PS beads consequently. Au mask is evaporated on the sample surface and tape stripped afterwards, leaving the hole-mask pattern, which is then developed in oxygen plasma. After nickel evaporation, the sample goes through acetone sonication, (lift off), which leaves the nickel nanodisks on the surface of the sample.

4.2   Fabrication of specific nanostructures for this thesis

As mentioned earlier, for the purpose of this project, nickel nanodisks of different sizes were used and, here I will explain how these samples were fabricated. Moreover, I will also briefly mention some other examples of nanostructures fabricated for associated work, which is not part of this thesis. All these samples were fabricated using the HCL method, but some of the parameters were altered to achieve desired shapes and thicknesses.

4.2.1   Nickel nanodisks

In my work, the main goal of using nanofabrication is to tune the LSPR frequency in nickel nanoparticles towards the intrinsic nickel interband transition region around 4.7 eV. This is possible by specifically adjusting the nickel disk diameter/thickness (i.e. the aspect ratio between diameter and thickness by either increasing diameter of the

PS beads while the thickness of the nickel evaporated is kept constant as well as the refractive index of the environment these nanodisks are embedded in. For tailoring the diameter of the nickel disks I simply used different sizes of PS particles, which resulted in different sizes of nanoholes after tape stripping, and eventually in different sizes of nickel disks on the sample surface. The PS nanoparticles used for the mask fabrication for this particular case had diameters of 40, 52, 60, 76, 110, 140, 170 and 190 nm.

For the purpose of changing the RI of the medium surrounding the nickel nanodisks to shift the resonance at constant disk geometry and volume, a 20 nm layer of SiO_2 was evaporated on to the sample to embed the nickel nanodisks. The latter increases the effective RI of the surrounding medium to a higher value of 1.5 compared to it's initial value RI (1.25) and results in red shift of LSPR related peak in the optical response of this sample towards the interband transition region. A schematic illustration of the used different nickel nanodisk designs as well as a SEM image of one of these samples is presented in figure 5.2.
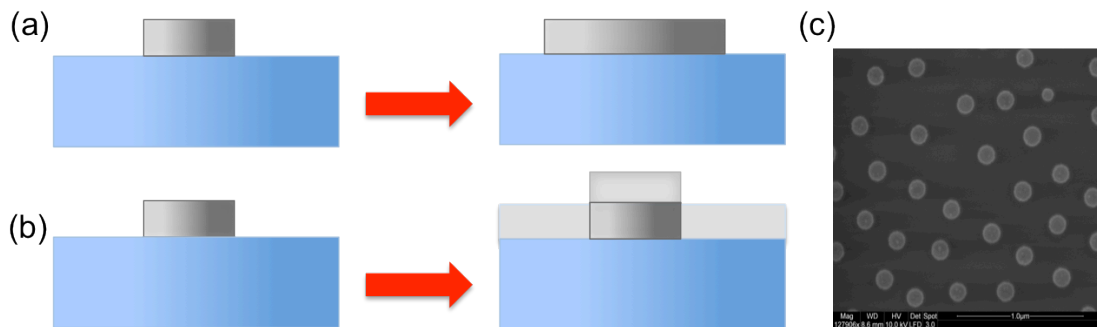

Figure 4.2: Schematic illustration of nickel nanodisk design by changing the diameter (a), thickness (b) and RI of the surrounding medium (c). SEM image of nickel nanodisks with diameter of 140 nm and thickness of 20 nm.

4.2.2   Nickel nano-ellipses

Similar to nickel nanodisks one can produce elongated structures such as ellipses just by tilting the sample holder during the hole-mask evaporation step in HCL. The latter results in elliptical holes in the hole-mask, rather than circular ones, due to the shadowing effect of the PS nanoparticles. The size of the ellipses will depend on the diameter of the PS particles used, as well as the tilt angle during mask evaporation (larger tilt = more elongated particles). The short axis of the ellipse will correspond to the diameter of the used PS particle, while the long axis length is dictated by the tilt angle. For the specific sample fabricated for a paper not included in this thesis, I fabricated nano-ellipses with short axis of 190 nm and long axis of 300 nm. Figure 5.3 presents the schematic drawing of the made elliptical structure as well as an SEM image of this specific sample.
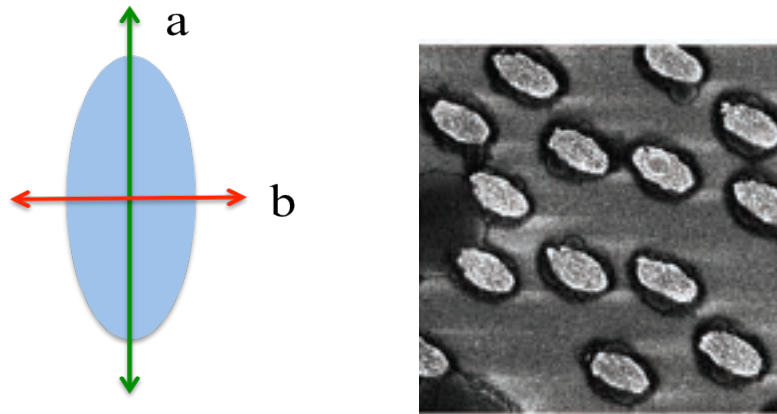
Figure 4.3: Schematic depiction of a nickel nano-ellipse with a showing the long axis and b representing the short axis. SEM image of nickel nano-ellipses with short axis of 190 nm and long axis of 300 nm.

5 Characterization

In the nanoplasmonics research field, to measure the optical properties of materials and plasmonic nanostructures, we usually investigate the interaction between these structures and incoming light. The latter is the fundamental basis of conventional spectrophotometry. However, in order to investigate the structural appearance, i.e. take an image of how the plasmonic nanostructure looks like in reality, conventional optical microscopes cannot be used due to (too) small sizes of the structures (below diffraction limit). This is why, instead, electron microscopy plays an important role in imaging plasmonic particles. In this chapter, I will first discuss the fundamentals of spectrophotometry and give a brief introduction of the spectrophotometer used for far-field characterization of the plasmonic nanostructures of interest. In the second part, scanning electron microscopy is introduced.

5.1 Spectrophotometry

Spectrophotometry is a tool to monitor the interaction between light and a plasmonic sample in order to investigate the optical properties of that specific sample. The spectrophotometer used for the purpose of characterization in this thesis is a Varian Cary 5000 (5.1) which is comprised of a light source, a monochromator, a sample holder and two light detectors (one for the UV-Vis and a second one for the NIR spectral range), as schematically depicted in Figure 5.2.a.

Figure 5.1: Varian Cary 5000 spectrophotometer together with the computer and software set for calculation of transmission, absorption and extinction.

The light irradiated from the light source passes through a diffraction grating, which, by being rotated in a step-wise fashion, produces monochromatic illumination, which can sweep the entire UV-Vis-NIR spectral range. Hence, in this spectrophotometer, one can measure the light-sample interaction each wavelength at a time. After the monochromator, the light hits the sample, where it is absorbed, scattered or transmitted in forward direction.

(a) lamp Monochromator Sample UV-Vis Detector NIR Detector
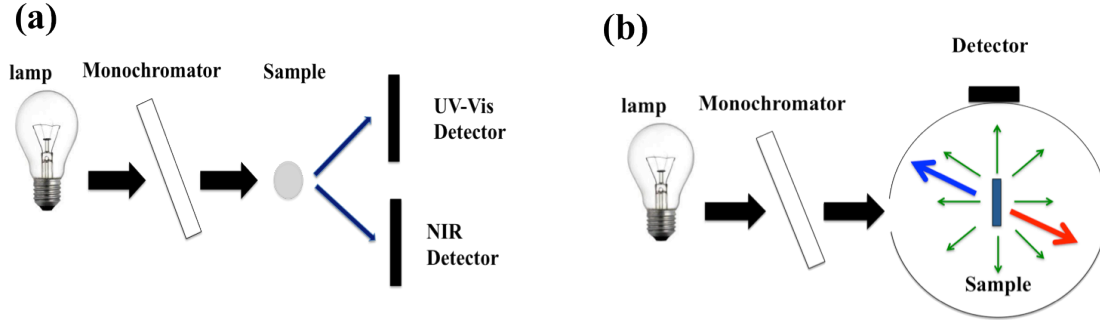
(b) lamp Monochromator Detector Sample

Figure 5.2: Schematic of transmission based (a) and absorption-based spectrophotometry using Cary Varian 5000. In transmission based spectroscopy the transmitted light through the sample is collected by the detectors and used for deriving the extinction spectrum. In absorption based spectroscopy the light reflected (blue arrow), transmitted (red arrow) and scattered (green arrows) by the sample that is located in the middle of the integrating sphere is collected by the detector, yielding an absorption spectrum [20].

The transmitted light is then collected by the detector and analyzed as a function of wavelength. The so-called transmittance of light through the sample as a function of wavelength can then be calculated by taking the ratio between the intensity of light impinging on the sample (I_0) vs. the intensity of the light detected at the detector after interaction with the sample (I), as shown in equation 5.1.

$$T = \frac{I}{I_0} \tag{5.1}$$

The transmittance is related to optical extinction through

$$E = 1 - T \tag{5.2}$$

Furthermore, since we know that light upon interaction with a material is either transmitted, scattered or absorbed, the sum of these should be equal to one. So we have

$$A + T + S = 1 \tag{5.3}$$

$$E = A + S \tag{5.4}$$

To measure the fraction of light absorbed by the sample (instead of transmitted as described above), an integrating sphere accessory to the Cary 5000 spectrophotometer can be used. In brief, the key asset of the integrating sphere is the high reflectivity of the surface of a sphere-shaped detector (up to 99%), which efficiently collects all transmitted and scattered light from a sample positioned in the sphere center (Figure 5.2.b). From an integrating sphere measurement absorption is calculated by

$$A = 1 - \frac{I}{I_0} \tag{5.5}$$

22

where I is the intensity of the incoming light and I_0 is the intensity of the light detected at the integrating sphere detector. On the other hand, from Beer-Lambert law we have

$$T = e^{\alpha l} = e^{-\sigma l N} \tag{5.6}$$

where α is the absorption coefficient and l is the path that light passes through in the material, σ is the absorption cross-section and N is the density (number per unit volume) of absorbing particles. From equations 5.1-5.6, we can obtain experimental absorption, extinction and scattering cross-sections.

Figure 5.3.a shows an example of experimentally measured extinction, scattering and absorption spectra for nickel nanodisks with diameter 60 nm and thickness of 30 nm. Figure 5.3.b contains the corresponding analytically calculated (by MLWA – see chapter 2 for more details) spectra for an oblate nickel spheroid with long axis 60 nm and short axis 30 nm. The qualitative agreement is very good.
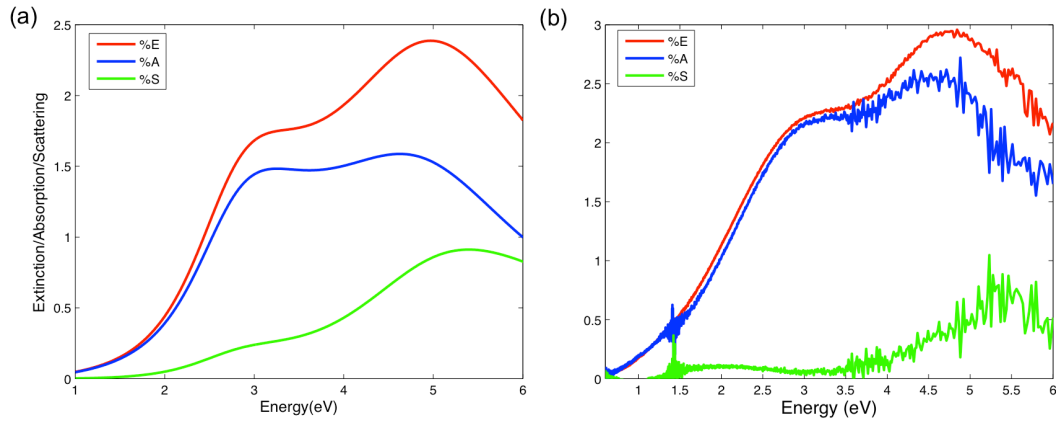

Figure 5.3: Extinction, absorption and scattering for nickel oblate spheroids (nanodisks) of diameter 60 nm and thickness of 30 nm. a) Calculations based on DL model and MLWA and b) experimentally measured spectrum by integrating sphere.

5.2 Scanning electron microscopy (SEM)

In order to see how samples actually look like in reality we need to image the nanostructures in some way. As conventional optical microscopes are limited to the light diffraction limit, we need to use a microscope that can go beyond this limit to be able to image nano-sized structures. Electron microscopy opens the door to imaging these particles and thus is one of the most well known techniques used for characterization and imaging of nanostructures in the plasmonic field.
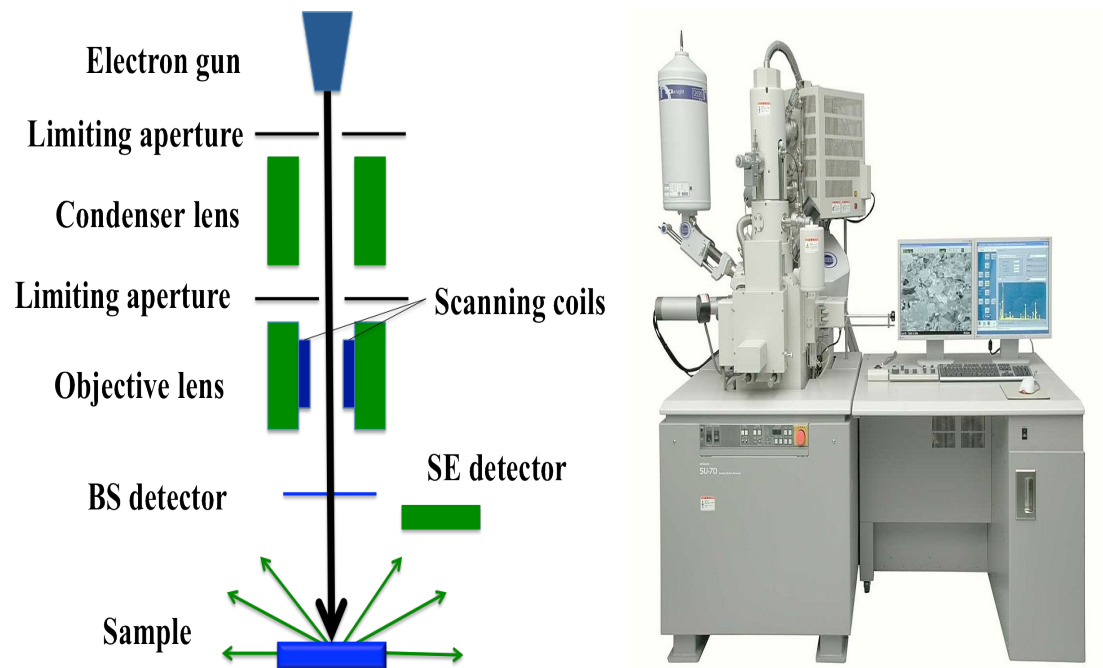

Figure 5.4: Schematic drawing of the scanning electron microscope optics with all its components to the left. Picture of a typical scanning electron microscope to the right.

In electron microscopy, as suggested from its name, electrons (instead of light) interact with the sample, and are thus used for "imaging". A focused electron beam is scanned over the sample and the electrons collected from this interaction are used to create the image of the sample [44]. A depiction of SEM electron optics as well as a picture of how this instrument looks is presented in figure 5.4.

In scanning electron microscopy, the electron beam scans the surface of the sample in a raster pattern and the electrons emitted back from the sample surface are analyzed for each "pixel". Two types of electrons are produced and analyzed: (i) So-called backscattered electrons, which are the result of elastic scattering of the probe electron beam from the sample. (ii) Secondary electrons, which are the result of inelastic scattering of the primary electron beam. Based on which type of electrons that are analyzed one can obtain different kinds of information about the sample. Backscattered electrons have the same energy as the primary electron beam due to elastic scattering. The number of backscattered electrons depends on the atomic number of the structure, i.e. heavier elements (higher atomic number) backscatter the electron beam more effectively than lighter elements (lower atomic number), which is why these electrons are used to detect contrast in materials with different chemical compositions and also the reason that heavier elements such as gold or nickel look brighter in SEM images compared to lighter elements like SiO_2. However, secondary

electrons are the result of inelastic scattering of the incoming electron beam, which means the incoming beam loses energy inside the material when colliding with sample atoms and this energy can be transferred to the electrons of the sample itself. Since this energy is much lower compared to the primary electron beam energy, it is only high enough for the electrons from the surface to escape from material and hit the detector but the electrons from deeper layers inside the sample cannot make it to the surface and are scattered along the way. The combination of the data gathered from the secondary and backscattered electron detectors provides us therefore with a detailed image of structure topography as well as chemical composition of the materials used in fabrication of the sample [44,45].

Although SEM is a valuable tool for imaging nanostructures, it has its own drawbacks. When it comes to imaging structures that are fabricated on non-conducting substrates such as silicon or fused silica, which I typically used in my work, the electron beam tends to build up negative charge on the specimen. This results in an electrical potential that deflects the electron beam from the scanned point and makes it almost impossible to achieve a high-resolution image of the structures with a conventional SEM. Fortunately, there is another type of SEM that makes it possible to image non-conducting substrates and even live/natural/bio samples that need to be kept humid during the imaging process. Specifically, this is done by using a so-called environmental scanning electron microscope (ESEM). Such instruments can operate (due to differentially pumped electron optics) in a water vapor background during imaging, which neutralizes the charges from the imaging electron beam and, hence, makes imaging of non-conducting substrates possible [46]. The images of nickel disks in this project were taken by ESEM.

6 Summary and outlook

In the appended paper, in order to explore the interaction between the plasmon resonance and the interband transition in the optical response of nickel nanostructures, I used two different approaches. The first approach was based on tuning the LSPR energy in nickel nanodisks via engineering the geometry of the particles. This was achieved by using different sizes of polystrene beads in the hole-mask colloidal lithography-based fabrication of the disks. The thickness was kept constant. In the second approach I used the sensitivity of LSPR to the refractive index of the surrounding medium to tune the LSPR peak in the optical response of nickel nanodisks with identical geometry. This was done by evaporating a thin layer of silica on top of the nickel nanodisks.

We made the following key observations: There are two distinct peaks in the far-field optical response of nickel nanodisks – one at low and one at high photon energies. Decreasing the size of the nickel nanodisks results in decreasing extinction efficiency of the low energy peak in the optical response, whereas the high energy peak extinction increases. Both peaks also shift to higher energies as the disk size is decreased. These experimental results are well reproduced using a Drude-Lorentz model along with modified long wavelength approximation (MWLA) to calculate the dielectric function of nickel and extinction/absorption/scattering efficiencies of nickel nanodisks, respectively. Of particular interest was the role of the interband transition at 4.7 eV in bulk nickel, which is defined by the band structure. This means that it is not expected to change by varying the geometry of nickel nanodisks in the size range considered (i.e. no quantum effects expected). However, as mentioned above, we observed two peaks, which *both* spectrally shifted upon engineering of the nickel disk size or it's dielectric environment. As we show in the appended paper this observation can be explained in a simple coupled harmonic oscillator model, which indicates that the LSPR and IBT in nickel nanodisks are a coupled system if their energies overlap. The coupled system has two new eigenfrequencies and exhibits a characteristic fingerprint of an *energy anticrossing* region. In this coupled regime with the distinct frequency split the LSPR and IBT "switch places", i.e. the IBT stays put around the constant value of 4.7 eV while LSPR shifts to higher energies - beyond the forbidden anticrossing range - with decreasing nanodisk diameter.

My study mainly focused on nickel as a model for other transition metals with interband transitions in the UV-VIS range. However, since the nickel interband transition is localized in the Deep-UV range, it was quite difficult to study the optical properties of nickel nanodisks above 6 eV. Therefore, metals such as Al, Co and Fe with lower IBT energies are definitely worth to investigate, specifically in the coupled regime.

I also investigated the amount of enhancement in the optical absorption of nickel nanoantennas imposed by the presence of the LSPR. Based on an approach developed in my project, the antenna enhancement factor on optical absorption could be derived by dividing the absorption efficiency of nickel nanodisks by the imaginary part of the dielectric function of nickel and the particle volume. We found the enhancement effect to be largest for small nickel disks. This enhancement phenomenon might be of interest for hot electron pair formation or heating in catalysis and photovoltaics [47].

7 Acknowledgment

There are some people whom without their help and support I wouldn't have accomplished so far and I would like to express my gratitude:

First, I would like to thank my examiner and co-supervisor Mikael Käll, for both your scientific and mental support, all hours of discussion on interband transition, antenna factor, writing and more serious talks on life matters. I will definitely take all of it with me.

I would like to thank my supervisors, Christoph and Sascha.

> Christoph, for all the time you put to read my licentiate and all your useful comments, finding time for me even when you were really busy, taking my supervision and helping me finalize the paper. It was really my pleasure to work with such a curious and self-driven and humble scientist.

> Sascha, for your supervision, time and effort to help me get into the nanoplasmonics field and teaching me all fabrication and characterization techniques and spending lots of time in the lab with me during my first year. Thank you for giving me the opportunity to peruse my academic career as a researcher.

Peter Apell, for all your valuable advice, for being such a modest and patient teacher and for opening my eyes to see all aspects of life. I will never forget what I learned from our talks and I'm really thankful to have met such a wonderful person in my life.

Julie and Helen, thank you for your positive attitude and all the support towards finishing my thesis.

Vladimir, for your collaboration and scientific discussions on calculation methods and helping me out with MLWA calculations.

Tavakol, for your collaboration and all your work on FDTD calculations.

Lianming, for helping me in the first months of my PhD to simply figure out what it was all about.

Björn, Robin, Timur, Si and Mokhtar, for all lunch/dinner/coffee breaks we shared and for making it more fun inside and outside Chalmers.

Kristofer, for being a nice office-mate. For tolerating heated office in cold winters and answering my various mac related questions whenever they popped out.

Olof, I always enjoyed your positive company, fun hours of different games specially the joyful moments of victory!

Carl and Mike, you honestly proved me real deep self-less friendship still exists. I cannot start to tell you how much you have helped me through this journey. All long walks, talks, fikas, fun and games, all your mental support and simply being there for

me kept me going. You have definitely added a new perspective to my life, which I will embrace forever. I'm deeply grateful for your wonderful friendship.

Laleh, I know I'm never alone cause I always have you right with me. All my life there was never even a single moment you were not there for me, always ready to sacrifice, always ready to be the strong one, always ready to give and never ask for anything in return. You are the sweetest kindest angel on earth and always have been and will be the closest to my soul.

Panti, for all your mental support and help during this time. You always made things look much easier, giving me motivation to go on when it was tough. Thanks for being such a wonderful caring sister.

Bogu, for your deep and unconditional love and support. For all the beautiful moments we share and for giving me the chance to experience true love. Thank you for keeping it always warm and cozy in my heart with your constant encouragement and believe in me. I'm lucky to have you and looking forward to all great adventures we will have in our life journey. Love you.

Finally, my parents for always believing in me, supporting me, loving me unconditionally, encouraging me to move forward and achieve my goals and for helping me simply to just be a better person in my life. I wouldn't have been here without your constant love and care.

8 Bibliography

[1] Faraday, M. "The Bakerian Lecture: Experimental Relations of Gold (and Other Metals) to Light." *Phil. Trans. R. Soc. Lond.*.147 (1857): 145-81.

[2] http://www.britishmuseum.org/explore/highlights/highlight_objects/ pe_mla/t/the_ly curgus_cup.aspx. (2013)

[3] Mie, G. "Beiträge Zur Optik Truber Medien, Speziell Kolloidaler Metallösungen." *Annalen Der Physik* 25.3 (1908): 377-445.

[4] Bohren, C.F and Huffman, D.R. "Absorption and Scattering of Light by Small Particles." *John Wiley and Sons, Inc., Germany* (1983).

[5] Yee, K. S. "Numerical Solution of Initial Boundary Value Problems Involving Maxwells Equations in Isotropic Media. Ieee Transactions on Antennas and Propagation." *Ap* 14.3 (1966): 302-07.

[6] Pennypacker, E. M. Purcell and C.R. "Scattering and Absorption of Light by Nonspherical Dielectric Grains." *Astrophysical Journal* 186.2 (1973): 705-14.

[7] Bonanni, V., et al. "Designer Magnetoplasmonics with Nickel Nanoferromagnets." *Nano letters* 11.12 (2011): 5333-8.

[8] Chen, J., et al. "Plasmonic Nickel Nanoantennas." *Small* (2011).

[9] Zoric, I.; Zach, M.; Kasemo, B.; Langhammer, C. *ACS Nano* 5 (2011): 2535–46.

[10] Hao, Q.; Juluri, B. K.; Zheng, Y. B.; Wang, B.; Chiang, I.-K.; Jensen, L.; Crespi, V.; Eklund, P. C.; Huang, T. *J. J. Phys. Chem. C* 114 (2010): 18059–66.

[11] Pakizeh, T.; Langhammer, C.; Zoric, I.; Apell, P.; Käll, M. *Nano Lett.* 9 (2009): 882–86.

[12] Johnson, P., and R. Christy. "Optical Constants of Transition Metals: Ti, V, Cr, Mn, Fe, Co, Ni, and Pd." *Physical Review B* 9.12 (1974): 5056-70.

[13] Palik, E. D. *Handbook of Optical Constants of Solids*. New York: Academic Press, 1991.

[14] Pakizeh, T.; Dmitriev, A.; Abrishamian, M. S.; Granpayeh, N.; Käll, M. *J. Opt. Soc. Am. B* 25 (2008): 659–67.

[15] Halas, N. J., et al. "Plasmons in Strongly Coupled Metallic Nanostructures." *Chemical reviews* 111.6 (2011): 3913-61.

[16] Optical Antennas." *Science* 308.5728 (2005): 1607-09. Pakizeh, Tavakol. "Optical Absorption of Plasmonic Nanoparticles in Presence of a Local Interband Transition." *The Journal of Physical Chemistry C* 115.44 (2011): 21826-31.

[17] Pakizeh, T.; Abrishamian, M. S.; Granpayeh, N.; Dmitriev, A.; Käll, M *Opt. Express* 14 (2006): 8240–46.

[18] Prodan, E., et al. "A Hybridization Model for the Plasmon Response of Complex Nanostructures." *Science* 302.5644 (2003): 419-22.

[19] http://en.wikipedia.org/wiki/Band_structure. (2013).

[20] Wadell, C. "Nanoplasmonics for Absorption Engineering and Hydrogen Sensing." (2012).

[21] http://en.wikipedia.org/wiki/Fermi_level. (2013).

[22] http://en.wikipedia.org/wiki/Band_gap. (2013).

[23] Potter, J.H. Simmons and K.S. "Optical Materials." *Academic Press, San Diego* (2000).

[24] Wooten, F. "Optical Properties of Solids." *Academic Press, New York* (1972).

[25] Phillips, J. C. "Fermi Surface of Ferromagnetic Nickel " *Phys. Rev* 133 (1964): 1020.

[26] Maxwell J. Mageto, C. M. Maghanga, and Mghendi Mwamburi. . "The Lorentz Oscillator Model Simulation Illustrating a Broad Maximum in the Bulk Reflectance

for Frequencies Just above the Resonance Frequency." *The African Review of Physics* 7:0011 (2012).

[27] http://en.wikipedia.org/wiki/Drude_model. (2013).

[28] Brian, B. "Plasmonic Nanostructures for Molecular Spectroscopy." (2011).

[29] Novotny, L.; Hecht, B. *Principles of Nanooptics*. New York: Cambridge University Press, 2006.

[30] Kelly, K. L.; Coronado, E.; Zhao, L. L.; Schatz, G. C. *J. Phys.Chem. B* 107 (2008): 668–77.

[31] M. Mayer , H. Hafner. "Localized Surface Plasmon Resonance Sensors." *Chem. Rev.* 111 (2011): 3828–57.

[32] E. Hutter , J. H. Fendle "Exploitation of Localized Surface Plasmon Resonance." *Adv. Mater* 16 (2004): 1685.

[33] F. Svedberg, Z. Li, H. Xu and M. Käll. "Creating Hot Nanoparticle Pairs for Surface-Enhanced Raman Spectroscopy through Optical Manipulation." *Nano Lett*, 6 12 (2006): 2639-41.

[34] P. Muhlschlegel, H. J. Eisler, O. J. F. Martin, B. Hecht and D. W. Pohl. "Resonant Optical Antennas." *Science* 308.5728 (2005): 1607-09.

[35] M. Meier, A. Wokaun. "Enhanced Fields on Large Metal Particles: Dynamic Depolarization." *Opt Lett* 8.11 (1983): 581-83.

[36] Fredriksson, H., et al. "Hole–Mask Colloidal Lithography." *Advanced Materials* 19.23 (2007): 4297-302.

[37] Jain, P. K.; Huang, X.; El-Sayed, I. H.; El-Sayed, M. A. *Acc. Chem.Res. 2008* 41 (2008): 1578–86.

[38] W. Sun, N. Loeb, Q. Fu "Finite-Difference Time-Domain Solution of Light Scattering and Absorption by Particles in an Absorbing Medium." *Appl. Opt.* 41 (2002): 5728-43.

[39] Lal, S.; Link, S.; Halas, N. *J. Nat. Photonics* 1 (2007): 641–48.

[40] Q. Fu , W. Sun. "Mie Theory for Light Scattering by a Spherical Particle in an Absorbing Medium." *Appl. Opt.* 40 (2001): 1354–61.

[41] Dasgupta, B. "Polarizability of Small Sphere Including Nonlocal Effect." *Phys. Rev. B* 24 (1981): 554–61.

[42] Novotny, L. "Strong coupling, energy splitting, and level crossings: A classical perspective. " *American Journal of Physics,* 78 .11 (2010): 1199-1202.

[43] H. W. Deckman, J. H. Dunsmuir. "Natural Lithography." *Applied Physics Letters*, 41.4 (1982): 377-79.

[44] http://en.wikipedia.org/wiki/Scanning_electron_microscope. (2013).

[45] G. I. Goldstein, D. E. Newbury, P. Echlin, D. C. Joy, C. Fiori, E. Lifshin. "Scanning Electron Microscopy and X-Ray Microanalysis." *New York: Plenum Press* (1981).

[46] Danilatos, G. D. "Theory of the Gaseous Detector Device in the Esem." *Advances in Electronics and Electron Physics. Advances in Electronics and Electron Physics* 78 (1990): 1-102.

[47] Hägglund, C.; Kasemo, B. *Opt. Express 2009* 17 (2009): 11944–57.